Materials Science & Engineering A 703 (2017) 293–303

Contents lists available at ScienceDirect

Materials Science & Engineering A

journal homepage: www.elsevier.com/locate/msea

Structure-properties relationship of ultra-fine grained V-microalloyed dual phase steels

C.P. Scott[a], F. Fazeli[a], B. Shalchi Amirkhiz[a], I. Pushkareva[a,*], S.Y.P. Allain[b]

[a] CanmetMATERIALS, 183 Longwood Rd S, Hamilton, Ontario, Canada L8P 0A5
[b] IJL, UMR CNRS-UL 7198, Parc de Saurupt, CS 50840, F-54011 Nancy Cedex, France

ARTICLE INFO

Keywords:
DP steels
AHSS
Ultra-fine grains
Vanadium microalloying

ABSTRACT

The effect of vanadium microalloying on ultra-high strength dual phase (DP) ferrite-martensite steel microstructure and properties was studied. It was found that the addition of 0.14 wt% V to a Fe-0.18C-1.5Mn-0.3Si-0.008N reference alloy introduced very significant ferrite grain size refinement in the cold rolled and annealed state. During continuous annealing the initial ferrite to austenite transformation kinetics were strongly retarded, however under slow cooling both pearlite and bainite transformations were suppressed indicating increased hardenability. After cold rolling and intercritical annealing at 750 ^{0}C intense V(C,N) precipitates (mean radius 3.7 nm) were observed in the ferrite phase whereas precipitates were scarce in martensite (austenite) and much larger (mean radius 6.7 nm). Significant gains in YS, UTS and work hardening rate were observed at low martensite fractions due to a combination of selective precipitation strengthening and grain refinement of ferrite. However, at higher martensite fractions (> 45%) the YS, UTS and work hardening rate became lower than the reference, primarily due to softening of the martensite. The latter was attributed to the fixing of solute carbon by V(C,N). The net increase in tensile strength with martensite content of the vanadium alloy was ~ 4 MPa/%α' compared to ~ 16 MPa/%α' for the reference alloy. A recently developed size-sensitive mean field structure-properties model was extended to capture these microalloying effects. At iso-tensile strength both the fracture strain and hole expansion behaviour of the new microalloyed steel showed improved performance over the reference.

1. Introduction

Advanced High Strength Steels (AHSS) are currently the fastest growing materials in the automotive body in white sector [1,2]. Their superior strength and formability allow direct substitution of older High Strength Low Alloy (HSLA) parts with reduced gauge components resulting in substantial weight savings at equivalent or improved functionality. Vehicle weight reduction and safety (crash) issues are driving the intensive AHSS development programs carried out by all major flat carbon steel manufacturers. The technology is evolving rapidly, with current strength targets moving beyond 1 GPa. In this region, many competing metallurgies exist and the best materials solutions are not yet known. Currently, the most widely implemented commercial AHSS products are dual phase (DP) ferrite-martensite cold rolled and annealed strips in the strength range 600–980 MPa, as recently reviewed by Tasan et al. [3]. Higher strength DP steels have been commercialized but further expansion of ultra-high strength (> 1 GPa) alloys is compromised by their rather mediocre damage resistance properties, especially in bendability and stretch flange forming operations [4]. The latter is usually simulated by the standard laboratory hole expansion (HE) test [5]. It is generally observed that the Hole Expansion Coefficient (HEC) of high strength steels decreases monotonically as the tensile strength increases, however DP steels do not follow this simple trend and can show unexpected variations in HEC as a function of the martensite content [6]. Improving the damage resistance (HEC and bendability response) of ultra-high tensile strength DP steels is thus a challenging objective for steel producers.

Depending on the specific DP microstructure, the most common damage initiation mechanisms in as-quenched alloys are martensite cracking and the nucleation of voids at ferrite-martensite interfaces [7,8]. Cracking is most evident in alloys with coarse grained or banded martensite whereas void formation followed by interphase decohesion is dominant for fine grained cold rolled and annealed microstructures. Decohesion is believed to be driven by strain incompatibilities between the soft ferrite and the hard martensite phases leading to the formation of voids at the phase boundaries [9]. Interestingly, if the material is tempered after quenching then interphase decohesion is suppressed and the dominant damage mechanism changes to decohesion at carbide/

* Corresponding author.
E-mail address: irina.pushkareva@canada.ca (I. Pushkareva).

http://dx.doi.org/10.1016/j.msea.2017.07.051
Received 29 May 2017; Accepted 17 July 2017
Available online 21 July 2017

martensite interfaces [10] and the HE properties are greatly improved, even though the tensile elongation decreases [9,10,12,13]. These tempering experiments clearly show that, for a constant martensite fraction, reducing the martensite strength, and hence reducing the initial ($\alpha'_{UTS}/\alpha_{UTS}$) ratio, strongly improves the HEC response. In practice post-quench tempering is not a favoured solution as it introduces a yield point with a Lüders plateau, it reduces the work hardening rate, tensile strength and uniform elongation and it increases production costs.

Some recent developments in DP design have focused on trying to improve damage resistance by modifying the strain partitioning between ferrite and martensite phases either by microstructure refinement [14] or by increasing the amount of metastable retained austenite (so called TRIP-assisted DP) [15]. An alternative strategy is investigated in this study – reduction of the ($\alpha'_{UTS}/\alpha_{UTS}$) ratio by selective strengthening of the ferrite phase using precipitation hardening. The approach is based on previous work by the authors on vanadium microalloyed Transformation Induced Plasticity (TRIP) ferrite + bainite + retained austenite steels [16,17] showing that it is possible, through the correct choice of composition and process parameters, to induce an intense distribution of intragranular V(C,N) precipitates that are localized in the ferrite phase during intercritical annealing of cold rolled strips. In this way, the austenite (martensite) phase is essentially unchanged whereas the ferrite phase is selectively strengthened. The following sections describe the results obtained on two laboratory alloys that were cast and processed on the pilot scale facilities at the CanmetMATERIALS laboratory (CMAT).

2. Experimental

Two alloys were cast into 55 kg ingots in a laboratory vacuum induction furnace and the measured compositions are shown in Table 1. The reference (*Ref*) alloy was designed using a recent structure-properties model for DP steels [18] to provide DP-1180 equivalent strength levels at much lower martensite fractions (40% α') than would normally be used for this grade in industry (> 70% α'). This explains the slightly higher than usual C content (0.186 wt%). No Cr or Mo additions were required as the quenching speeds used in this study were very high and the Al content was kept as low as possible to minimise AlN precipitation. The second alloy (*Ref + V*) has the same base chemistry with the addition of 0.14 wt% V. The nitrogen level is a little higher than most industrial DP grades (0.008 wt%) in order to promote V(C,N) precipitation. The same N content was used in the *Ref* steel to maintain parity in interstitial elements. These V and N contents were optimized to provide the most effective selective ferrite strengthening effect, based on previous experience with microalloyed TRIP steels [17].

The reheating, hot rolling, cooling and coiling parameters were designed to produce bainitic hot strips with the maximum amount of V maintained in solid solution before cold rolling. A detailed description of the processing strategy is given in [19]. The hot strips were cold rolled from 3 mm to 1 mm (66% reduction) under tension in 7 passes using the CMAT pilot rolling mill.

The phase transformation behaviour of full hard cold rolled strips was investigated in a Bahr DIL 805 dilatometer and a Gleeble 3800 simulator. Large area sheet annealing was done in specially adapted furnace with a thermal variation of ± 10 ^{0}C over an area of 100 mm × 100 mm. After annealing the sheets were directly quenched between flat dies in a Macrodyne 1200t press. Die quenching is advantageous as it provides high quenching rates (~ 200 ^{0}C/s) and eliminates the risk of sheet distortion introduced by water quenching. The transfer time between the furnace and the quench start was ~ 5 s. During this time the air cooling rate for the 1 mm sheet was ~ 15 ^{0}C/s. The phase fractions and grain sizes of the annealed strips were determined using optical microscopy and SEM imaging. Image analysis was carried out using the ImageJ software. The martensite content was determined on the basis of the average of 10 micrographs at × 1000 magnification (optical microscopy) or × 2000 (SEM). EBSD analysis was performed on an FEI Nova NanoSEM equipped with an OIM 6.2 EBSD system from EDAX. It was confirmed that the quenched microstructures consisted of ferrite and martensite and that the retained austenite volume fractions were < 1%. The fast quench rate ensured that no bainite was present. TEM studies were carried out on a Tecnai Osiris 200 kV FEG-STEM equipped with a Gatan Enfina EELS system and four windowless Super-X SDD EDX detectors for chemical mapping. Specimens were prepared from thin foils and from both direct and indirect extraction replicas. The tensile properties were determined using subsize ASTM E8/E8M specimens with a 25 mm gauge length and 6 mm width with the gauge length cut parallel to the sheet transverse direction. The strain rate was a constant 2 × 10^{-3}/s. Fracture strains were calculated from the reduction in area of broken tensile specimens. Three measurements were made on each specimen. Hole expansion tests were carried out on 100 mm × 100 mm coupons according to Ref. [5] using an automated testing rig with an integrated video crack detection system at ArcelorMittal Dofasco's R & D centre.

Table 1
Chemical compositions of the test alloys expressed in wt%.

Alloy	C	Si	Mn	V	N	Mo	Cr	Al
Ref	0.186	0.19	1.59	0.003	0.008	0.01	0.03	0.011
Ref + V	0.182	0.19	1.65	0.140	0.008	0.01	0.03	0.019

3. Results

3.1. Hot band microstructure and properties

The hot band microstructures and properties were previously described in [19] and will only be briefly summarized here. For both the *Ref* and *Ref + V* samples coiled at 500 ^{0}C the matrix consisted of a mixture of coarse bainite along with some carbide containing phases. Some evidence of microstructural refinement was seen in the *Ref + V* alloy. Film-like cementite particles were identified by TEM diffraction at grain and lath boundaries and EDX analysis confirmed that these cementite particles contained between 0.5 at% and 3.7 at% V. Tensile testing revealed that the hot band UTS increased from ~ 600 MPa to ~ 700 MPa due to the V additions. In addition to the grain boundary cementite some alignments of coarse intragranular particles ~ 50 nm in diameter were observed. TEM EDX chemical analysis confirmed that the intragranular particles were rich in V and N and it is most probable that these were strain induced nitrogen rich V(C,N) formed during the last passes of hot rolling. We can compute the expected *YS* increment in ferrite, ΔYS_P due to VN precipitation using the modified Ashby–Orowan relation proposed by Gladman [20];

$$\Delta YS_P = 0.538G\, b(f^{1/2}/X) \quad (1)$$

where G is the shear modulus in MPa (80 GPa at 20 °C), b is the Burgers vector in μm (2.5 × 10^{-4} μm), f is the volume fraction of V(C,N) precipitates and X is the mean particle diameter expressed in μm. The value of f cannot be reliably measured using TEM techniques but fortunately some data from selective chemical dissolution/ICPMS measurements on steels with similar composition and processing conditions is available in the literature. A reasonable assumption would be that no more than 13% of the total V content was precipitated in the hot band [17] in which case ΔYS_P would be + 17 MPa. Note that even if all of the V was precipitated in this form then the maximum strengthening contribution $\Delta YS_{P\ max}$ from these particles would be + 47 MPa. If precipitation strengthening is discounted then the change in hot band strength could reasonably be attributed to the action of solute vanadium in delaying the bainite transformation to lower temperatures, resulting in a refined microstructure with a higher fraction of lower bainite, as has recently been observed in lower C line-pipe steels [21].

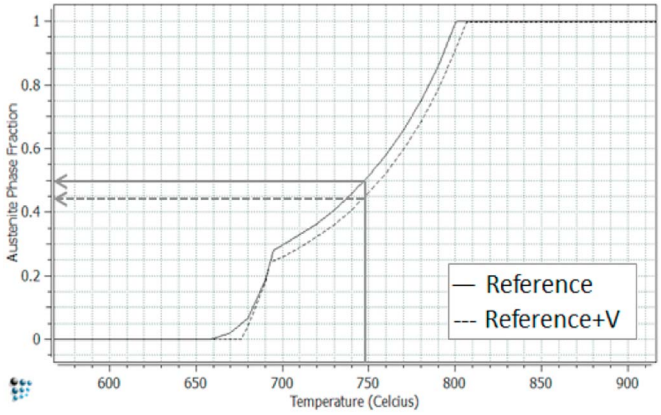

Fig. 1. Equilibrium phase fractions of austenite as a function of temperature calculated by MatCalc.

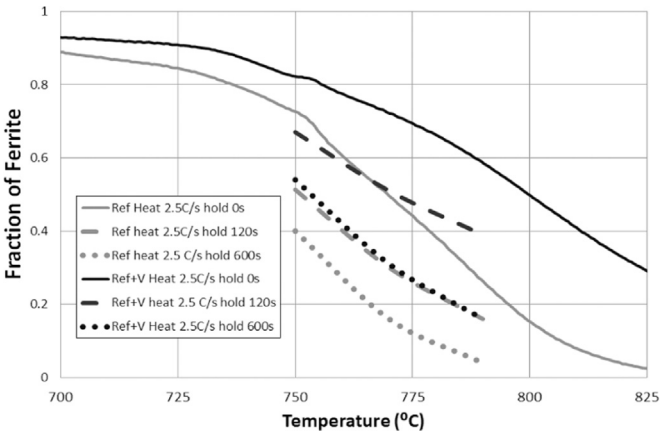

Fig. 2. Phase fraction of ferrite during heating and isothermal holding. Solid lines→ heating rate of 2.5 ^{0}C/s, broken lines→after isothermal holding for 120 s and 600 s.

3.2. Phase transformation behaviour

According to the MatCalc equilibrium calculation shown in Fig. 1, the addition of 0.14 wt% V to the *Ref* alloy should result in a slight increase in the Ae_3 temperature from 800 ^{0}C to 806 °C i.e. at an intercritical annealing temperature of 748 ^{0}C the equilibrium fraction of austenite should be 0.5 for the *Ref* alloy and 0.44 for the *Ref + V* alloy. The experimental data from Gleeble and Bahr dilatometry experiments on full hard cold rolled samples indicates that the phase transformation behaviour is dominated by kinetic effects (Fig. 2). At a constant heating rate of 2.5 ^{0}C/s (continuous lines) the *Ref* alloy starts to transform to austenite first (as expected). Isothermal holding for 2 min and 10 min at temperatures in the range 750–790 ^{0}C (dotted and dashed lines) indicates that the transformation is very sluggish in the *Ref + V* alloy i.e. under practical continuous annealing conditions the *Ref + V* alloy will always form significantly less austenite than the *Ref* alloy held at the same temperature. In fact to achieve the same austenite fraction in the range 750–790 ^{0}C the *Ref + V* sample must be soaked for 5 times longer.

A further experiment was carried out to check the effect of V on phase transformation during cooling. Fig. 3 contains raw dilatometry data for continuous heating of cold rolled full hard *Ref* and *Ref + V* samples at 2.5 ^{0}C/s to 790 ^{0}C, holding for 120 s (*Ref*) and 600 s (*Ref + V*) until ~ 85% austenite has formed and then air cooling (~ 10 ^{0}C/s to 700 ^{0}C then 4–6 ^{0}C/s to 500 ^{0}C). The difference in the kinetics of the ferrite to austenite transformation is very clear in this graph. The red arrow indicates the point where the phase fractions were checked (in a separate trial) by fast quenching – it was found experimentally that the *Ref* sample contained ~ 81% austenite and the *Ref + V* sample had ~ 77% austenite at this point. The blue arrows indicate the start of ferrite, pearlite and bainite transformations on cooling. As can be seen the austenite to ferrite transformation begins at a slightly higher temperature in the *Ref + V* alloy (in agreement with the equilibrium diagram (Fig. 1)) and it appears that the pearlite transformation is completely suppressed and that the bainite transformation is strongly retarded. Fig. 3b and c illustrate clearly the strong effect of V on cooling; the *Ref* sample microstructure is majority ferrite/pearlite with $HV_{0.5}$ = 189 whereas the *Ref + V* sample is dual phase (ferrite + auto-tempered martensite with traces of bainite) with $HV_{0.5}$ = 235. Thus, under air cooling conditions V additions promote ferrite formation but suppress pearlite and retard bainite so that the overall hardenability is increased – this observation is in agreement with the early reported behaviour of V in air-cooled DP steels [22]. Obviously this increased hardenability is a positive benefit for DP production on older annealing lines with limited fast cooling capability or for the production of thicker gauges (hot strips) where the cooling rate is non-uniform.

3.3. Microstructure of the annealed cold strips

A series of 24 continuous annealing trials were carried out on full hard cold rolled sheets at temperatures between 735 ^{0}C and 790 ^{0}C (Table 2). The annealing times were varied between 60 s and 180 s before die quenching the material to room temperature. The most striking observation is the high degree of microstructural refinement introduced by the vanadium additions. Fig. 4a and b are optical micrographs of the *Ref* and *Ref + V* alloys annealed at 750 ^{0}C for 120 s and 180 s respectively. With the Lepera etchant used here the martensite phase is white and ferrite is brown. The ferrite mean grain size was reduced by ~ 2.5 times in the *Ref + V* alloy (from 4 μm to 1.6 μm). Similar refinement was noted at intercritical temperatures up to 760 ^{0}C. Above this temperature martensite becomes the matrix phase and the difference in the ferrite grain size of the *Ref* and *Ref + V* alloys decreases.

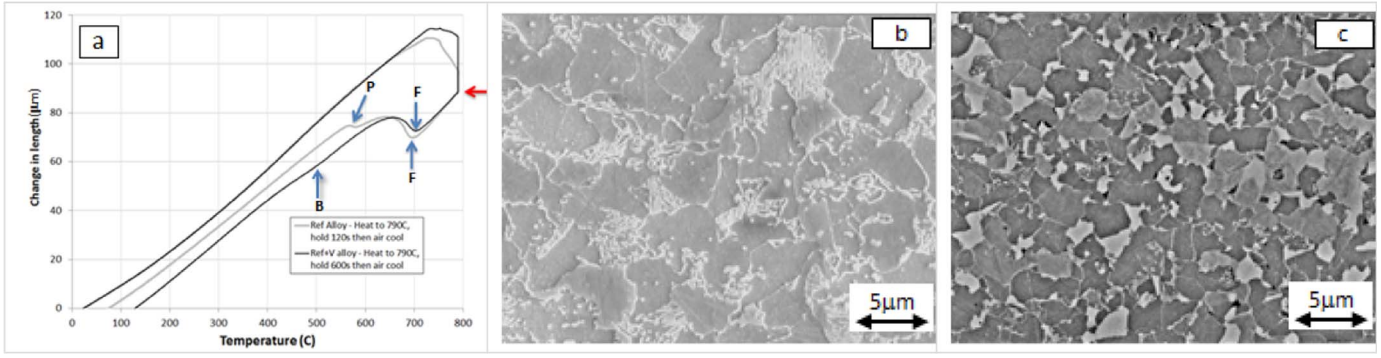

Fig. 3. a) Dilatometry data showing the phase transformations on continuous heating at 2.5 ^{0}C/s to 790 ^{0}C, holding for 120 s (Ref alloy) or 600 s (Ref + V alloy) until ~ 85% austenite has formed followed by natural air cooling. b + c) SEM images of the air cooled samples from Fig. 3a after Nital etching; b) Ref and c) Ref + V.

Table 2
Summary of the continuous annealing/die quenching experiments.

Alloy	Annealing temp (°C)	Annealing time (s)	Martensite fraction (%)	Ferrite grain size (μm)	YS (MPa)	UTS (MPa)	UE (%)	YS/UTS
Ref	740	60	11.5	6.5	403	704	9.8	0.57
Ref	740	120	21.0	5.0	426	749	8.8	0.57
Ref	740	120	29.0	4.1	468	930	9.9	0.50
Ref	750	120	30.0	3.9	542	1101	5.9	0.49
Ref	750	120	31.5	4.8	505	1015	7.6	0.50
Ref	760	120	38.0	6.6	536	1088	5.9	0.49
Ref	750	120	38.8	7.5	558	1094	4.6	0.51
Ref	760	120	47.4	4.5	580	1106	3.6	0.52
Ref	770	120	51.0	2.1	669	1341	7.0	0.50
Ref	770	120	52.0	2.4	697	1379	5.6	0.51
Ref	790	120	63.3	1.7	884	1467	5.5	0.60
Ref	790	120	71.4	2.9	854	1435	5.5	0.60
Ref + V	740	120	20.4	2.3	594	1099	7.2	0.54
Ref + V	740	60	21.0		559	1057	10.5	0.53
Ref + V	750	90	27.0	2.0	602	1145	7.2	0.53
Ref + V	750	180	28.0	1.6	629	1194	7.7	0.53
Ref + V	750	90	42.0	1.5	638	1193	7.9	0.53
Ref + V	760	120	45.9	2.5	593	1123	7.0	0.53
Ref + V	750	120	46.0	2.0	606	1146	6.6	0.53
Ref + V	750	180	52.0	1.6	642	1196	7.3	0.54
Ref + V	770	120	53.2	2.0	693	1280	5.0	0.54
Ref + V	760	90	57.0	1.8	651	1254	7.1	0.52
Ref + V	790	120	61.5	1.4	646	1243	6.4	0.52
Ref + V	780	120	67.0	1.4	750	1343	6.1	0.56

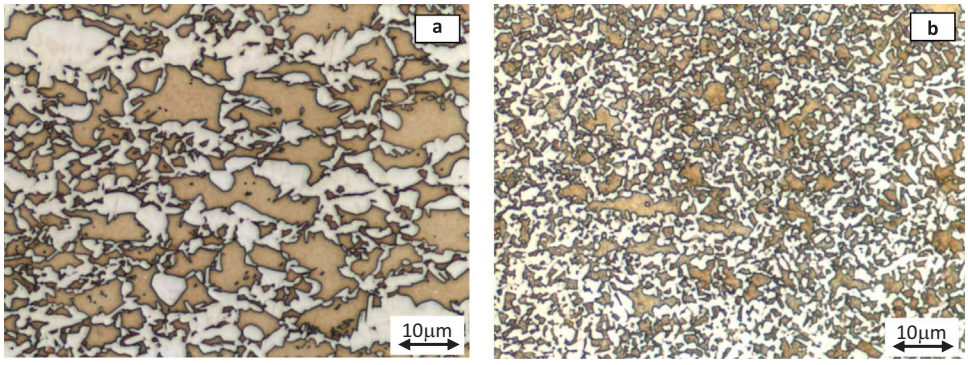

Fig. 4. Optical micrograph of the a) Ref alloy annealed at 750 °C/120 s, b) Ref + V alloy annealed at 750 °C/180 s. The martensite is white and ferrite is brown (Lepera etchant).

A bright field (BF) STEM image of the *Ref + V* alloy annealed at 740 °C/120 s is shown in Fig. 5a. Here, multiple austenite grains have nucleated around the central recrystallized ferrite grain. The austenite grains can easily be identified by the partitioning of Mn [23] as shown in blue in the EDX chemical map of Fig. 5b. In this image the mean Mn content in martensite is ~ 2.3 wt% and in ferrite ~ 1.3 wt%. A number of undissolved globular cementite precipitates 100–200 nm in diameter can be seen in the ferrite regions. The cementite observed in the hot strip had a very different film-like morphology indicating that spheroidisation occurred during the continuous annealing step. The globular cementite particles are strongly enriched in Mn (up to ~ 10 wt%) which greatly increases their stability. Undissolved Fe_3C precipitates were observed in both the *Ref* and *Ref + V* alloys at temperatures ≤ 740 °C and for annealing times up to 180 s. However, they were no longer present at 750 °C. The same behaviour was reported by Papa Rao et al. [24] for a DP steel with a much lower C content (0.12 wt%) which was

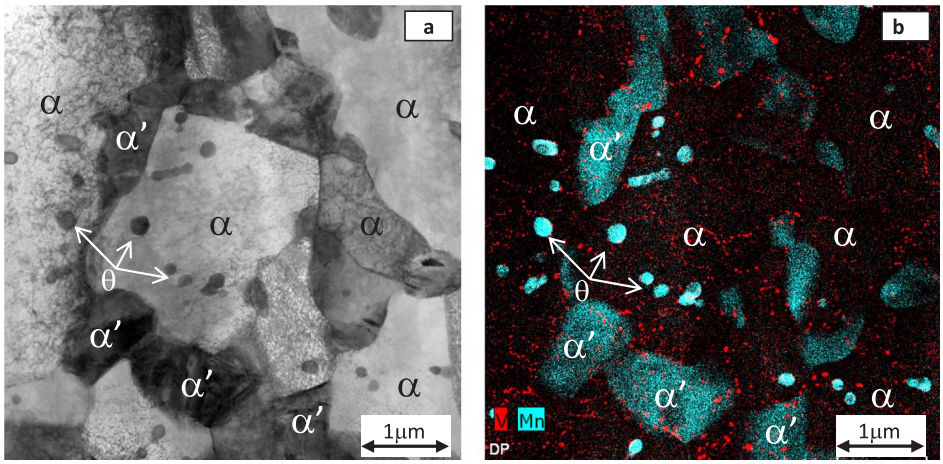

Fig. 5. a) Thin foil BF STEM image of the Ref + V alloy after annealing at 740 °C/120 s and die quenching. b) Composite EDX chemical map of the same region showing Mn (blue) and V (red). (For interpretation of the references to color in this figure legend, the reader is referred to the web version of this article.)

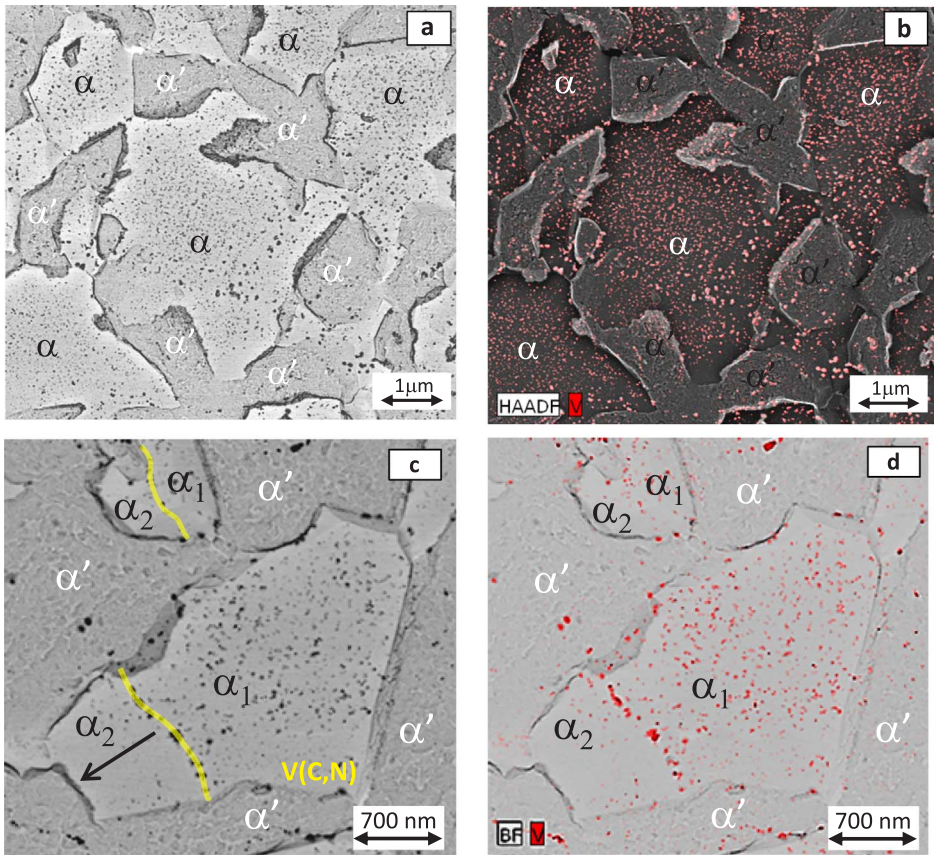

Fig. 6. a) BF STEM image of a direct extraction replica (Ref + V alloy annealed at 750 °C/180 s and die quenched), b) EDX chemical map superimposed on the HAADF image of a) (note reversed contrast) showing the localisation of V precipitates (red) in ferrite. c) BF STEM image showing primary (untransformed) ferrite islands (α_1) which have grown into austenite (regions α_2) by reverse transformation during air cooling before quenching. d) EDX chemical map showing the V distribution in c). (For interpretation of the references to color in this figure legend, the reader is referred to the web version of this article.)

cold rolled and annealed from a starting ferrite/pearlite hot band microstructure. The EDX map in Fig. 5b also shows the distribution of intragranular V precipitates (in red) in the foil. While there are V-containing particles in both phases, it is clear that the highest number density occurs in the ferrite.

The Fe_3C particles in Fig. 5b appeared to be a favoured nucleation site for V(C,N) precipitates adding further proof that the latter must also have nucleated and grown during continuous annealing. The carbon content of the martensite islands in the *Ref + V* sample annealed in a salt bath at 735 °C for 90 s and water quenched was measured using Electron Energy Loss Spectroscopy (EELS) in the TEM [25]. Six martensite islands were investigated and the carbon concentrations varied widely between 0.34 wt% and 1.03 wt% with an average of 0.7 ± 0.22 wt% From Fig. 1 the equilibrium martensite fraction in this sample should be 38% so that equilibrium austenite carbon composition should be ~ 0.48 wt% thus confirming the dilatometry data that the ferrite → austenite phase transformation did not reach equilibrium in the *Ref + V* alloy.

The V(C,N) precipitate distribution was studied quantitatively using direct carbon extraction replicas i.e. the carbon film is directly evaporated onto the previously lightly etched sample surface and then separated chemically. This technique is especially well adapted to the extraction of the very smallest precipitates. An example is shown in Fig. 7 where the smallest extracted V(C,N) particles that were reliably identified by EDX mapping (arrowed) are only 2 nm in diameter. One disadvantage with the direct method is that precipitates are extracted from a volume (and not a surface), thus the smallest particles tend to agglomerate on the replica. This requires manual intervention during image analysis to determine the particle size distribution. Returning to the question of the distribution of V particles, Fig. 6a shows a STEM

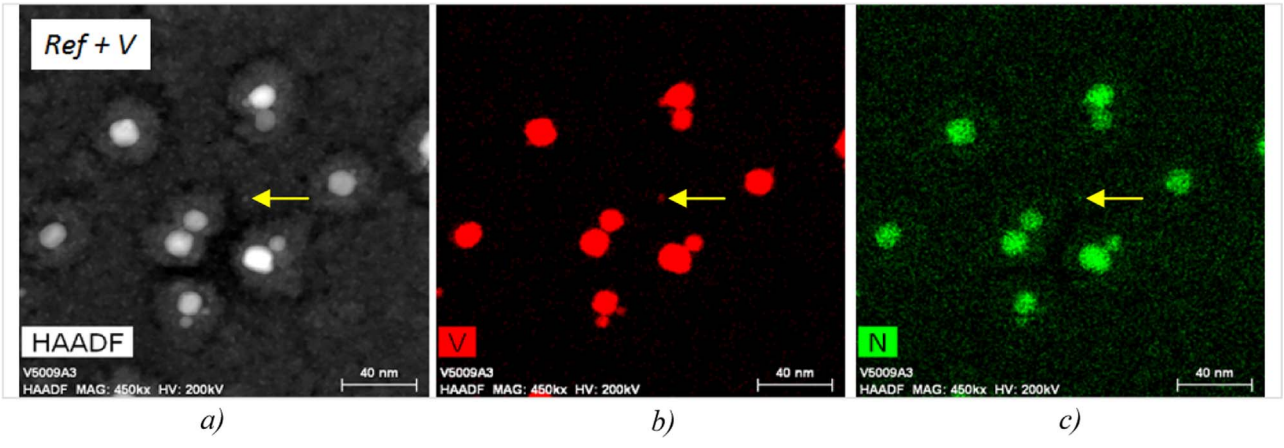

Fig. 7. a) HAADF STEM image of a direct extraction replica from the Ref + V alloy after annealing at 750 °C/180 s showing clustering of very small V(C,N) particles. b) V map. c) N map. The arrows indicate a 2 nm diameter V(C,N) precipitate.

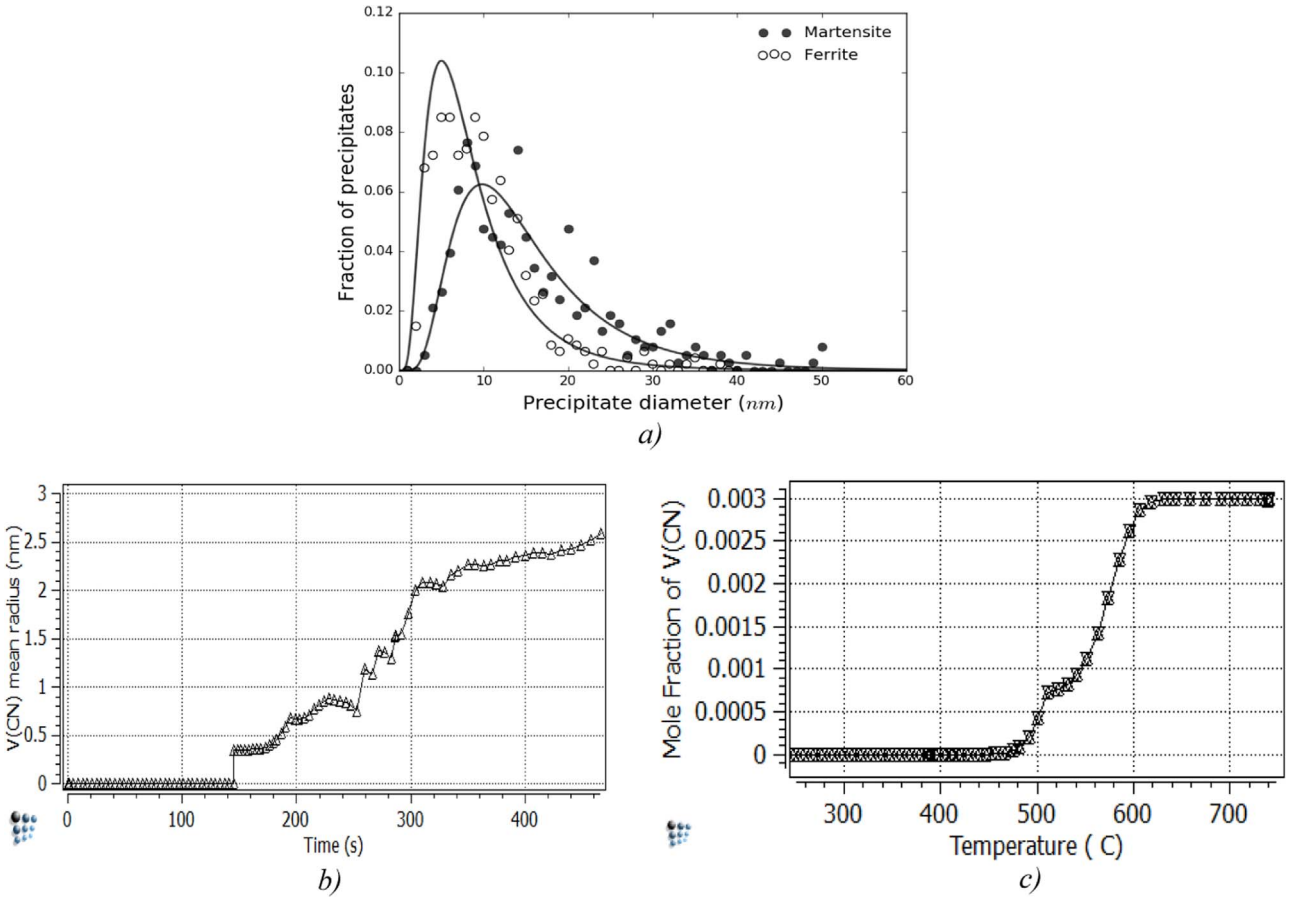

Fig. 8. a: V(C,N) size distributions in ferrite and in martensite for the Ref + V alloy after annealing at 750 ^{0}C/180 s (heating rate ~ 2.5 ^{0}C/s). b: calculated V(C,N) mean radius in ferrite during annealing at 750 ^{0}C/180 s (heating rate 2.5 ^{0}C/s). c: calculated mole fraction of V(C,N) precipitated during annealing at 750 ^{0}C/180 s (heating rate 2.5 ^{0}C/s).

bright field image of a direct replica extracted from the *Ref + V* alloy annealed at 750 ^{0}C/180 s and die quenched. The darker (thicker) regions of the replica show the martensite phase, and the lighter (thinner) regions indicate ferrite. At this temperature all the cementite particles were dissolved. Again a high density of intragranular precipitates is visible in ferrite. The EDX map in Fig. 6b confirms that these are vanadium precipitates and that they are very heavily (but not exclusively) concentrated in ferrite.

The V precipitates are not completely uniformly distributed inside the ferrite grains, For example, Fig. 6c and d show one ferrite grain where there are two distinct regions separated by an alignment of larger V precipitates. The most likely explanation for this is that, at the end of isothermal annealing the ferrite/austenite boundary was positioned at the large particles (note that it was often observed that the V particles at grain boundaries were coarser than the intragranular precipitates). Slow air cooling occurs during the transfer period just before quenching causing the boundary to move from the original position such that the ferrite grain grows into the austenite, as indicated by the arrow. Assuming this interpretation is correct then the precipitates cannot be acting to inhibit the movement of the austenite-ferrite interface, in contradiction to the mechanism proposed by Ballinger and Gladman [26]. The newly transformed ferrite region (which we will call secondary ferrite) must inherit the same precipitate distribution (and Mn content) as the parent austenite and so it will be much softer than the primary ferrite but still stronger than the ferrite in the *Ref* steel.

The precipitate size distributions for the *Ref + V* alloy following annealing at 750 ^{0}C/180 s were determined in ferrite (579 particles measured) and in martensite (380 particles measured). Lognormal distributions were fitted to the data (Fig. 8a) and it was found that the weighted mean particle diameter was ~ 7.4 nm in ferrite and ~ 13.4 nm in martensite. The mean precipitate diameter in martensite is comparable to that reported by Perrard [17] in a study on TRIP steels intercritically annealed for 180 s at the slightly higher temperature of 775 ^{0}C. However, the ferrite particle diameter is significantly smaller here, 7.4 nm compared with 15 nm in [17]. A kinetic simulation of V(C,N) precipitation in ferrite was carried out for the same thermal cycle using the MatCalc code (Fig. 8b and c) assuming nucleation on the dislocations from cold rolling. The calculated mean V(C,N) diameter at the end of annealing was ~ 5.2 nm and all of the V was precipitated at 620 ^{0}C i.e. during the heating ramp.

3.4. Mechanical properties of annealed cold strips

The cold strip mechanical properties were investigated in the as-quenched state by tensile testing and by hole expansion trials. The tensile curves can be seen in Fig. 9a and b and the YS and UTS are plotted as a function of martensite fraction in Fig. 9c and d. The fracture strain and HEC are shown as a function of the tensile strength in Fig. 9e and f. The uniform elongation showed a lot of scatter (Table 2) and it was not possible to distinguish any significant difference between the two steels. A recent mean-field size-dependent structure-properties model for non-microalloyed DP steels [18] was used to calculate the YS and UTS of the *Ref* alloy. The model takes as inputs the chemical composition, the martensite fraction and the ferrite mean grain size (see Table 2). It can be seen from Fig. 9c and d that the predicted values of YS and UTS show excellent agreement with experiment and the trends are well reproduced. The experimental data from the *Ref* alloy shows a linear increase in UTS of ~ 16 MPa/%α' up to about 55% martensite fraction where saturation begins. These results are quite compatible with published DP data [27]. On the other hand, the *Ref + V* alloy

presents a completely different and somewhat unexpected tensile behaviour. At martensite fractions ≤ 40% both the YS and the UTS are higher than the *Ref* material. However, beyond this point the *Ref + V* samples are actually softer than their *Ref* counterparts. A further difference is that no clear saturation in UTS was observed. The net effect is that the dependence of both the YS and UTS on martensite fraction is reduced by a factor of 3–4 times, to ~ 4 MPa/%α' for the latter. Similar behaviour for hot rolled DP strips with Ti [28] and V [29] additions has been mentioned in the literature.

The expected *YS* increment ΔYS_P due to V(C,N) precipitation can be calculated using Eq. (1) assuming that the effect of precipitation strengthening in as-quenched martensite is negligible [30]. From Fig. 8c the kinetics of V(C,N) formation in ferrite are very fast. Evaluating Eq. (1) for the *Ref + V* alloy annealed at 750 ^{0}C/180 s using X = 7.4 nm and assuming that all of the nominal 0.14 wt% V is precipitated as V(C,N) (volume fraction $f = 0.00263$) gives $\Delta YS_P = +75$ MPa. The increment in the ferrite YS introduced by decreasing the grain size from 5 μm to 2 μm is + 58 MPa [18] so that the total change in the yield stress due to V additions is ~ + 133 MPa. This is comparable to the increase in YS at low martensite fractions (Fig. 9c).

It has been reported that there is an experimentally observed correspondence between tensile fracture strain and HEC values [10,11], however the correlation is not unique and contains a microstructure dependence component [10]. The fracture strains of both alloys are plotted against tensile strength in Fig. 9e and the corresponding HEC data is shown in Fig. 9f. The error bars in Fig. 9f show the maximum and minimum UTS values from tensile specimens cut from the annealed sheets adjacent to the HEC coupons. It is not correct to directly compare Fig. 9e with Fig. 9f as there is a wide variation in the microstructures, however the general trends are very similar. The fracture strain and HEC of the *Ref* alloy decrease rapidly with tensile strength (martensite fraction) to a minimum which occurs at ~ 1050 MPa (corresponding to ~ 33%α') for this material. This is very close to the critical volume fraction for percolation (0.29) when martensite islands in a ferrite matrix are considered to be random overlapping ellipsoids of revolution with aspect ratios between ~ 0.5 and ~ 2 [39]. Then there is a plateau extending to ~ 1350 MPa (55% α') whereupon there is some improvement in both RA and HEC as the matrix tends to single phase martensite. This behaviour is similar to that reported previously by the authors [10]. It is interesting to note that the improvement in HEC occurs at nearly the same martensite fraction as the start of the saturation in UTS.

4. Discussion

4.1. Microstructure and phase transformation behaviour

The effect of V additions on the microstructure and phase transformation behaviour is complex. Firstly there is a very strong refinement of the hot and cold strip microstructures (especially the latter) which appears to be a common observation for DP steels microalloyed with V [17,32], V + Nb [24], Ti [28] and Nb [31]. However, the reduction in the ferrite grain size observed here is greater than reported elsewhere (Fig. 4). The reasons for this are not obvious - vanadium is not believed to show a strong solute drag effect and does not retard recrystallization in austenite to the same extent as Nb and Ti. One major difference is that, due to its high solubility in austenite and the fast cooling/low coiling temperature processing route, most of the V in the *Ref + V* steel precipitates during annealing after cold rolling. V(C,N) nucleates on dislocations during the heating stage of continuous annealing (Fig. 8c) and the precipitate number density is actually highest just before the first austenite starts to form [17]. These precipitates strongly retard the growth of any newly recrystallized ferrite grains in the *Ref + V* steel by Zener pinning. Compared to the *Ref* alloy annealed under the same conditions, this will result in either a higher density of smaller recrystallized ferrite grains (at slow heating rates) or a higher fraction of unrecrystallised ferrite (at fast heating rates). In both cases the available grain boundary surface for austenite nucleation is increased.

The second effect of V is to strongly delay the formation of austenite during heating and isothermal holding (Fig. 2) and to promote the reverse transformation to ferrite during cooling while at the same time retarding/suppressing the pearlite and bainite transformations i.e. it provides an overall increase in hardenability. Looking first at the cooling behaviour, after intercritical holding the austenite to ferrite transformation temperature is slightly higher in the *Ref + V* alloy due to thermodynamic effects (Fig. 1). This is technologically important as many commercial continuous annealing lines have a transfer zone between soaking and the start of quenching or fast cooling where secondary ferrite can form. This secondary ferrite could have an important influence in V microalloyed DP as it is softer than the primary ferrite (it inherits the precipitate distribution in austenite – Fig. 6d) and, depending on the amount that is formed, could affect both the initial yielding response and possibly the damage behaviour by acting as a favoured initiation site. The suppression of pearlite by V additions has been observed by other workers [22,26,29] and it has been suggested that it is related to the strong refinement in the austenite grain size [26] however no reason was given for this. The effect of V in delaying the bainite transformation is more subtle and is the subject of current research [21,33].

Turning to the heating cycle, it is clear that the model for austenite nucleation and growth proposed by Huang et al. [34] does not apply to either the *Ref* or *Ref + V* alloys processed in this study as the first (primary) austenite will nucleate at individual spheroidised cementite precipitates rather than in extended pearlite colonies. The number density and size of these particles will be similar for both alloys. This cementite is located at the grain boundaries of unrecrystallised ferrite or inside recrystallized ferrite grains (Fig. 5a). During austenite nucleation both the recrystallized ferrite fraction and grain size should be smaller in the *Ref + V* alloy, but the density of primary nucleation sites (cementite) will be similar in both alloys. It is hard to imagine a mechanism involving growth competition between primary austenite and grain boundary nucleated austenite which will *reduce* the overall austenite growth kinetics in a refined ferrite matrix with a lower recrystallized ferrite fraction. The difference in the austenite growth kinetics is therefore more likely to be associated with some change in the diffusivity of carbon in ferrite. This could be a direct effect due to the competition for carbon between V(C,N) and growing austenite, or a significant change in the carbon diffusion coefficient caused by the presence of solute V. Clearly more work is required in this area.

4.2. Work hardening and damage behaviour

The evolution of the strain hardening and work hardening response of the *Ref* and *Ref + V* steels with martensite content is plotted in Fig. 10a–d. From the strain hardening data (Fig. 10a and b) all of the specimens tested followed the Considère criterion and ruptured very quickly after the onset of plastic instability (except *Ref* 38% and *Ref + V* 42% martensite which appeared to show premature fracture). Beyond 2% straining, the instantaneous strain hardening exponent decreases with increasing martensite content, however the effect appears to be much smaller for the *Ref + V* steel. A further difference is that the tendency to form a distinct yield point in the lower martensite fraction *Ref* samples is partially suppressed in the *Ref + V* steel. This could be indicative of C-V interactions that reduce or retard the formation of Cottrell atmospheres on mobile dislocations (GNDs) in ferrite and merits further study.

The work hardening data (Fig. 10c and d) shows a marked influence of the V additions – compared to the *Ref* sample the work hardening rate of the *Ref + V* alloy is higher at low martensite fractions and lower at high martensite fractions i.e. it is compressed, becoming much less sensitive to the martensite content. This explains the UTS crossing

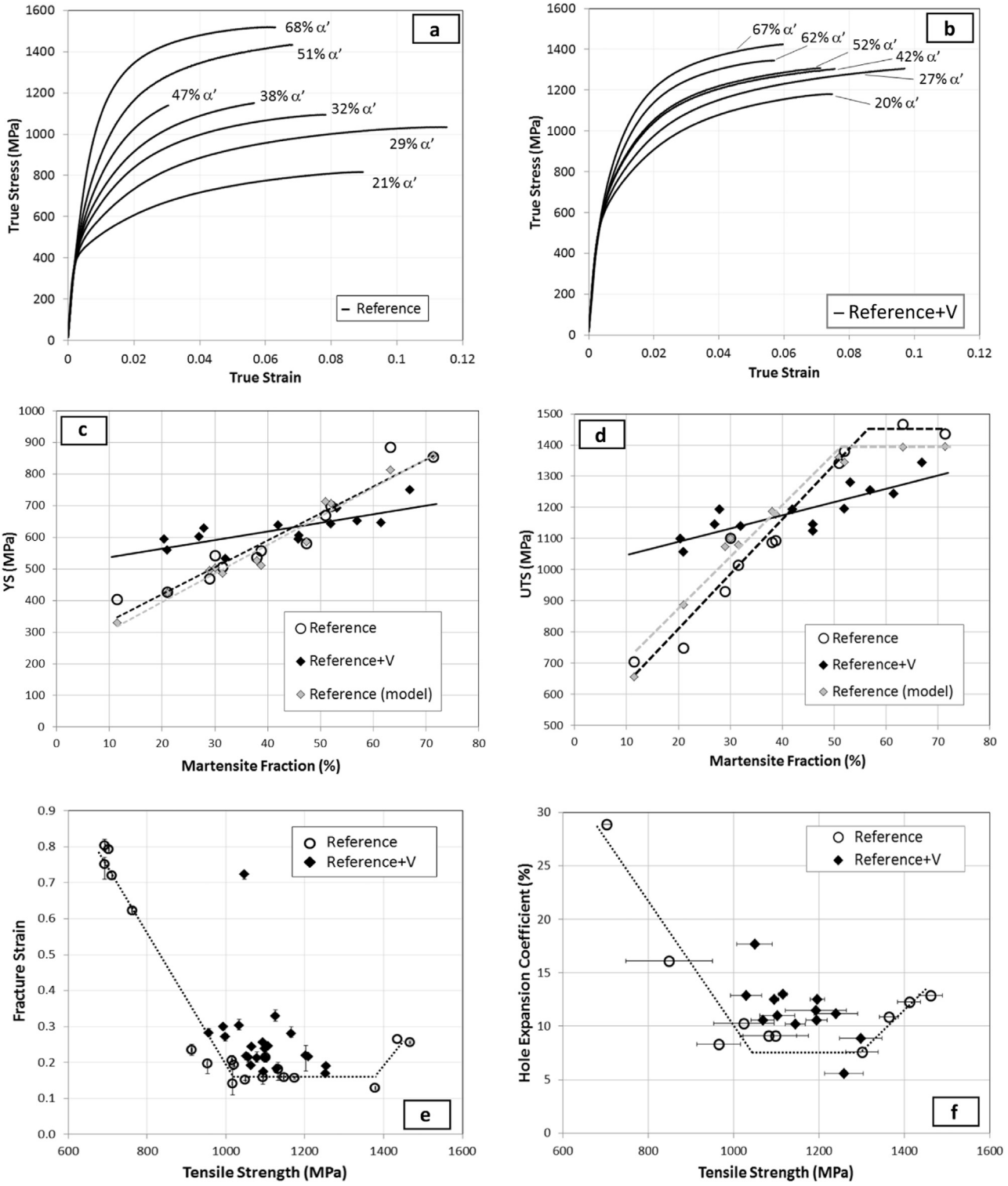

Fig. 9. Mechanical properties of the Ref and Ref + V alloys; a) + b) true stress v true strain data c) + d) YS and UTS plotted as a function of martensite fraction, e) + f) fracture strain and Hole expansion coefficient plotted as a function of UTS.

behaviour in Fig. 9d – at low martensite fractions the ferrite in the *Ref + V* alloy is strengthened by V(C,N) and by grain refinement and the work hardening rate is much higher so there is large increase in UTS (> 300 MPa). However, the work hardening rate and the yield stress of the *Ref* alloy increase faster with martensite content and converge with the *Ref + V* steel at ~ 40% α' and 45% α' respectively. This could be due to two factors; 1) the difference in the ferrite grain sizes decreases as the volume of martensite increases and 2) the martensite in the *Ref + V* sample is softened by the competition for C from V(C,N) precipitates. Here it should be noted that the kinetic of cementite dissolution may also play an important role at annealing temperatures below 750 ^{0}C (martensite fractions < ~ 25%). Clearly as the yield strength and work hardening rate are similar the UTS's must converge in this martensite range.

At martensite fractions above 45% both the YS and the work hardening rate of the *Ref + V* alloy are inferior to the *Ref* steel and

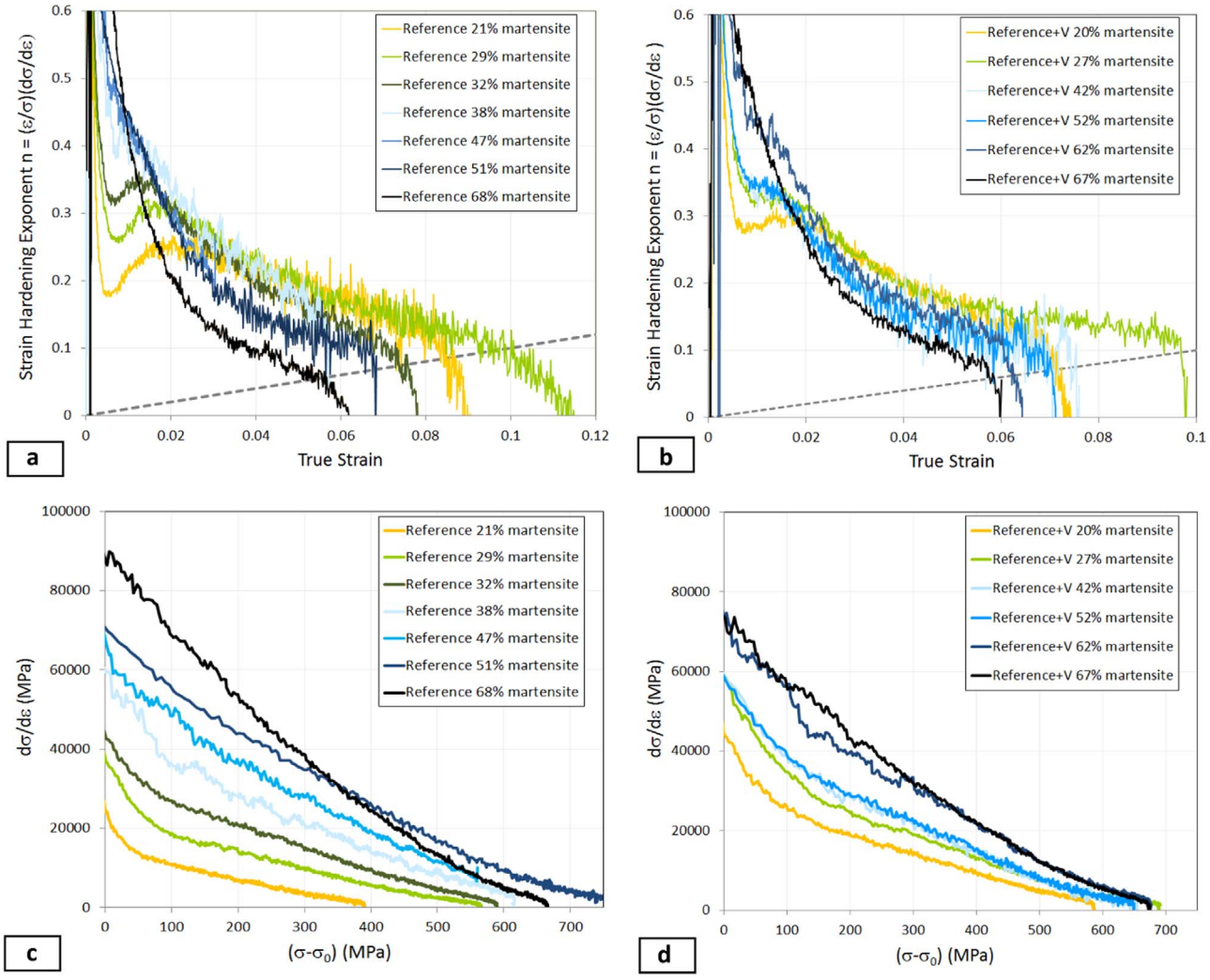

Fig. 10. Evolution of the strain hardening exponent n of a) Ref and b) Ref + V alloys with martensite fraction. Work hardening plotted against flow stress for c) Ref and d) Ref + V alloys for different martensite fractions.

logically the UTS is also lower. The reason for this must lie in the martensite phase; as ferrite becomes the minority phase the ferrite grain sizes in the *Ref* and *Ref + V* steels converge (Table 2) and the influence of precipitation strengthening may be diminished by coarsening, but the *Ref + V* ferrite can never become softer than the ferrite in the *Ref* steel. If we assume as an upper bound that all of the Vanadium in *Ref + V* is precipitated as VC then the solute carbon content will be reduced by 0.033–0.149 wt%. The decrease in the martensite yield stress due to this loss of carbon in solid solution can be estimated from the work of Roberts and Owen [35] as:

$$\Delta\sigma = Mm(\Delta X_c)^{1/2} \quad (2)$$

where X_c is the atom fraction of carbon, M is the Taylor Factor and $m = 0.051\mu$ ($\mu = 80$ GPa is the shear modulus). Applying this formula gives $\Delta\sigma_{max} = -107$ MPa when taking $M = 3$. This result is comparable with the observed difference in YS (and UTS) at high martensite fractions.

Concerning the work hardening behaviour, many authors have reported an increased work hardening as the ferrite grain size is reduced [14,26,31,36,37]. This is generally attributed to an earlier onset of plastic deformation in the martensite phase as ferrite deformation is restricted due to the decrease in the mean free path for dislocation gliding. Further, the increase in the ferrite/martensite interface area results in a higher density of GNDs in ferrite produced both during the martensitic transformation and by subsequent straining. These GNDs generate an unrelaxed internal back stress which contributes to kinematical hardening [18]. Finally, Kamakawa et al. [32] observed a significant increase in work hardening of DP steels with VC precipitates that they attributed to enhanced dislocation multiplication caused by the precipitates. The effect disappeared for martensite fractions ≥ 50%. This claim must be interpreted with caution as the grain size of their reference steel (35 μm) was twice as large as the VC containing alloy (16 μm). However, given that these grain sizes are both coarse the majority of the extra work hardening contribution may really be due to VC. At higher martensite fractions the contribution from ferrite decreases and the work hardening behaviour becomes dominated by martensite. The single biggest factor in martensite plasticity is the interstitial carbon content [35] so it is highly likely that the work hardening rate of the *Ref + V* alloy drops below that of the *Ref* steel because some carbon is consumed in V(C,N) precipitates. The combined effect results in a "compression" of work hardening with martensite fraction (Fig. 10a and b).

A complete structure-properties description of the *Ref + V* alloy would require coupling a kinetic precipitation model to capture the dissolution of cementite and the nucleation and growth of V(C,N) in ferrite and austenite together with a phase transformation model. This is beyond the scope of the present work. In order to test the basic ideas of ferrite strengthening and martensite softening the mean-field model of Allain [18] was modified as follows:

The flow stress σ^f of ferrite was rewritten as:

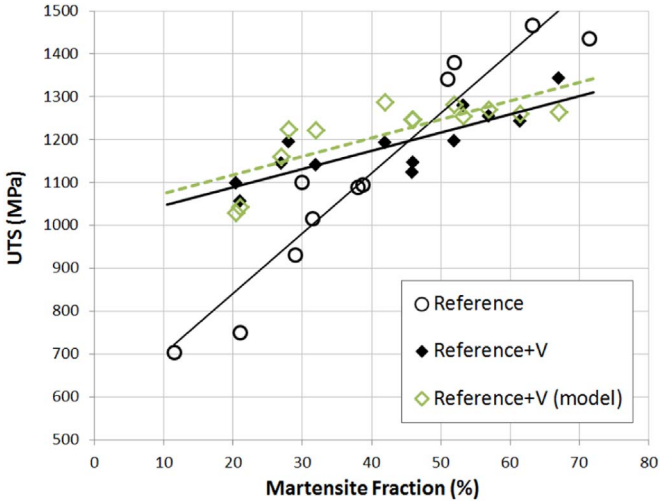

Fig. 11. Application of the modified mean field DP structure-properties model to the Ref + V alloy.

$$\sigma^f(\varepsilon_f^p) = [(\sigma_0^f)^2 + (\Delta YS_p)^2]^{1/2} + \sigma_R^f + \sigma_X^f \quad (3)$$

where σ_0^f is the friction stress, σ_R^f is a classical isotropic Taylor forest dislocation hardening term and σ_X^f is a kinematical hardening contribution. The calculation of these terms is documented in [18]. ΔYS_p is the precipitation strengthening term given by Eq. (1).

The description of martensite was not changed except to subtract the carbon content from VC precipitation (in ferrite and austenite):

$$\%C_m = \frac{\%C_0 - \%C_{VC}}{F_m} \quad (4)$$

where C_m is the martensite carbon content, C_0 is the nominal carbon concentration, C_{VC} is the total amount of carbon precipitated with vanadium (in ferrite and in austenite) and F_m is the martensite fraction. A comparison of the model calculated UTS with the experimental data for the *Ref + V* alloy can be seen in Fig. 11. Here a number of simplifying approximations were made for all martensite fractions:

- the ferrite grain size was fixed to be 2 μm,
- the mean VC precipitate diameter was fixed at 7.4 nm (i.e. the measured diameter in ferrite),
- all of the V was assumed to precipitate as VC.

In spite of these approximations the model (shown as the dotted line in Fig. 11) manages to capture the most important trends of the *Ref + V* experimental results i.e. the alloy is stronger than the *Ref* steel at low martensite fractions, becomes softer at higher (> 50%) martensite content and overall the dependence of the UTS on martensite content is greatly reduced.

Turning to the damage behaviour the fracture strain and HEC results are well correlated and indicate that the *Ref + V* steel performed better in these tests i.e. it does show better damage resistance properties than the *Ref* alloy, however the gains are quite modest. Many authors have suggested that the $(\alpha'_{UTS}/\alpha_{UTS})$ ratio is the controlling parameter for good HEC performance [7,9,10,38] and that refining the ferrite grain size has a positive effect [37]. While there is clear experimental evidence for the beneficial effects of softening martensite by tempering on HEC in DP steels [9,10,13] the available literature data on the benefits of strengthening ferrite is less convincing. The results of this study (Fig. 9e, f) do go some way to confirm the $(\alpha'_{UTS}/\alpha_{UTS})$ hypothesis but it does seem that the potential gains are small compared to the much larger improvements in RA and HEC that can be obtained by tempering. It is possible that the gains have been reduced by the presence of softer, secondary ferrite (Fig. 6d) but this is unlikely to have much influence at low martensite fractions. Another possibility is that the presence of a high density of nano-precipitates in ferrite changes the damage behaviour. Further investigations including nano-indentation and in-situ DIC to study strain partitioning and damage initiation are in progress.

5. Conclusions

The effect of vanadium microalloying on the microstructure and properties of a high strength dual phase steel was studied. Compared to the Fe-0.186C-1.5Mn-0.3Si-0.008N reference alloy it was found that the addition of 0.14 wt% V resulted in:

- A very significant ferrite grain size refinement in the cold rolled and annealed state. It is proposed that this is due to Zener pinning of newly recrystallized ferrite by V(C,N) precipitates nucleated on dislocations during the heating portion of intercritical annealing.
- During continuous annealing the initial ferrite to austenite transformation kinetic was strongly retarded, possibly due to a competition for carbon between austenite nuclei and growing V(C,N) precipitates
- On slow cooling after intercritical annealing the ferrite start transformation temperature was slightly increased but the pearlite and bainite transformations were suppressed, resulting in a net overall increase in hardenability.
- Undissolved cementite was observed at intercritical annealing temperatures ≤ 740 ^{0}C.
- After annealing at 750 ^{0}C/180 s intense V(C,N) precipitation (mean diameter 7.4 nm) was observed in the ferrite phase whereas precipitates were scarce in martensite (austenite) and much larger (mean diameter 13.4 nm).
- The increase in tensile strength with martensite fraction of the reference alloy (~ + 16 MPa/%α') was well predicted by a recent microstructure/properties model. The vanadium alloy was much stronger than the reference steel at low martensite fractions due to grain refinement and selective strengthening of the ferrite phase. However, for α' > 45% it actually became softer than the reference steel. The net result was that the vanadium alloy showed a much lower sensitivity to martensite content (~ 4 MPa/%α').
- The work hardening rate of the vanadium alloy was higher than the reference at low martensite fractions (due to ferrite grain size refinement and precipitation strengthening) but became lower for martensite fractions > 40% as the influence of ferrite decreases and the martensite carbon content is reduced through competition with V(C,N).
- At iso-tensile strength the fracture strain and hole expansion coefficient of the V alloy showed some improvement over the reference steel, however the gains were much smaller than those obtained by tempering.

Acknowledgements

The authors are grateful to John Hilbert, David Milbourn and the Vanitec Technical committee for supporting this work. Prof. H. Zurob provided invaluable assistance with annealing trials and Dr J. Gao at ArcelorMittal Dofasco carried out the HEC testing. The authors would also like to thank the LABEX DAMAS (ANR-11-LABX-008-01) from Lorraine, France for their support. Finally, we wish to acknowledge the help and professionalism of the staff at CanmetMATERIALS who participated in this study.

References

[1] O. Bouaziz, H. Zurob, M. Huang, Driving force and logic of development of advanced high strength steels for automotive applications, Steel Res. Int. 84 (10) (2013) 937–947.
[2] B. Zuidema, Bridging the design–manufacturing–materials data gap: material properties for optimum design and manufacturing performance in light vehicle steel-intensive body structures, JOM 64 (9) (2012) 1040–1047.

[3] C.C. Tasan, M. Diehl, D. Yan, M. Bechtold, F. Roters, L. Schemmann, C. Zheng, N. Peranio, D. Ponge, M. Koyama, K. Tsuzaki, D. Raabe, An overview of dual-phase steels: advances in microstructure-oriented processing and micromechanically guided design, Annu. Rev. Mater. Res. 45 (2015) 391–431.
[4] T. Senuma, Physical metallurgy of modern high strength steel sheets, ISIJ Int. 41 (6) (2001) 520–532.
[5] ISO/TC 164/SC 2, Hole Expanding Test, ISO, Geneva, 2006.
[6] I. Pushkareva, C.P. Scott, M. Goune, N. Valle, A. Redjaimia, A. Moulin, Distribution of carbon in martensite during quenching and tempering of dual phase steels and consequences for damage properties, ISIJ Int. 53 (7) (2013) 1215–1223.
[7] G. Avramovic-Cingara, C.A.R. Saleh, M.K. Jain, D.S. Wilkinson, Void nucleation and growth in dual-phase steel 600 during uniaxial tensile testing, Metall. Mater. Trans. A 40A (2009) 3117–3127.
[8] E. Maire, O. Bouaziz, M. DiMichiel, C. Verdu, Initiation and growth of damage in a dual-phase steel observed by X-ray microtomography, Acta Mater. 56 (2008) 4954–4964.
[9] K. Hasegawa, K. Kawamura, T. Urabe, Y. Hosoya, Effects of microstructure on stretch-flange-formability of 980 MPa grade cold rolled ultra high strength steel sheets, ISIJ Int. 44 (2004) 603.
[10] I. Pushkareva, S. Allain, C.P. Scott, A. Redjaïmia, A. Moulin, The relationship between microstructure, mechanical properties and damage mechanisms in high martensite fraction dual phase steels, ISIJ Int. 55 (10) (2015) 2237–2246.
[11] T.M.Link, G.Chen, Anisotropy effects of axial crash behaviour of advanced high-strength steels, in: Proceedings of International Symposium on New Developments in AHSS, Vail, 2013, p. 63.
[12] J. Kang, Y. Ososkov, J.D. Embury, D.S. Wilkinson, Digital image correction studies for microscopic strain distribution and damage in dual phase steels, Scr. Mater. 56 (2007) 999–1002.
[13] A. Kamp, S. Celotto, D.N. Hanlon, Effects of tempering on the mechanical properties of high strength dual-phase steels, Mater. Sci. Eng. A 538 (2012) 35–41.
[14] Q. Lai, O. Bouaziz, M. Goune, A. Perlade, Y. Brechet, T. Pardoen, Microstructure refinement of dual-phase steels with 3.5% Mn: influence on plastic and fracture behaviour, Mater. Sci. Eng. A 638 (2015) 78–89.
[15] B.L. Ennis, E. Jimenez-Melero, E.H. Atzema, M. Krugla, M.A. Azeem, D. Rowley, D. Daisenberger, D.N. Hanlon, P.D. Lee, Metastable austenite driven work-hardening behaviour in a TRIP-assisted dual phase steel, Int. J. Plast. 88 (2017) 126–139.
[16] C.P.Scott, P.Maugis, P.Barges, M.Goune, Microalloying with vanadium in TRIP steels, in: International Conference on Advanced High Strength Sheet Steels for Automotive Applications – Proceedings, Winter Park, Colorado, USA, June 6–9, 2004, pp. 181–193.
[17] F. Perrard, C.P. Scott, Vanadium precipitation during intercritical annealing in cold rolled TRIP steels, ISIJ 47 (8) (2007) 1168–1177.
[18] S. Allain, O. Bouaziz, I. Pushkareva, C.P. Scott, Towards the microstructure design of DP steels: a generic size-sensitive mean-field mechanical modelling, MSEA A 637 (2015) p222–p234.
[19] C.P.Scott, F.Fazeli, B.Shalchi, I.Pushkareva, Properties of ultra-fine grained V-microalloyed dual phase steels, in: Proceedings International Symposium on New Developments in Advanced High Strength Sheet Steels, Keystone Colorado, 30th May–2 June, 2017.
[20] T. Gladman, Precipitation hardening in metals, Mater. Sci. Technol. 15 (1) (1999) 30–36.
[21] F.Fazeli, C.P.Scott, B.Shalchi, M.Arafin, S.Nafisi, L.Collins, R.Glodowski, Bainite Formation and Softening in Vanadium Containing Line Pipe Steels, Presented at MS & T, Oct 4–8, Columbus, Ohio, 2015.
[22] P. Ostrom, B. Lonnberg, I. Lindgren, Role of vanadium in dual-phase steels, Met. Technol. (1981) 81–93.
[23] S. Sun, M. Pugh, Manganese partitioning in dual phase steel during annealing, Mater. Sci. Eng. A 276 (2000) 167–174.
[24] M. Papa Rao, V. Subramanya Sarma, S. Sankaran, Microstructure and mechanical properties of V-Nb microalloyed ultrafine-grained dual-phase steels processed through severe cold rolling and intercritical annealing, Metall. Mater. Trans. A 48A (2017) 1176–1188.
[25] C.P. Scott, J. Drillet, A study of the carbon distribution in retained austenite, Scr. Mater. 56 (6) (2007) 489–492.
[26] N.K. Ballinger, T. Gladman, Work hardening of dual phase steels, Met. Sci. (1981) 95–108.
[27] R.G. Davies, Influence of martensite composition and content on the properties of dual phase steels, Metall. Trans. A 9A (1978) 671–679.
[28] C.-N. Li, X.-L. Li, G. Yuan, R.D.K. Misra, J. Kang, G.-D. Wang, Precipitation behaviour and mechanical properties of a hot-rolled Ti-bearing dual phase steel, Mater. Sci. Eng. A 673 (2016) 213–221.
[29] A. Hansson, R. Lagneborg, A. Melander, The influence of annealing procedure on the mechanical properties of a C-Mn and C-Mn-V dual phase steel, Scand. J. Metall. 4 (1983) 177–183.
[30] F.B. Pickering, High-Strength, Low-Alloy Steels – A Decade of Progress, Microalloying'75, Union Carbide Corp., New York, NY, 1977, p. 9.
[31] A. Ghatei Kalashami, A. Kermanpur, E. Ghassemali, A. Najafizadeh, Y. Mazaheri, Correlation of microstructure and strain hardening behaviour in the ultrafine-grained Nb-bearing dual phase steels, Mater. Sci. Eng. A 678 (2016) 215–226.
[32] N. Kamakawa, M. Hirohashi, Y. Sato, E. Chandiran, G. Miyamato, T. Furuhara, Tensile behaviour of ferrite-martensite dual phase steels with nano-precipitation of vanadium carbides, ISIJ Int. 55 (8) (2015) 1781–1790.
[33] F.Fazeli, C.P. Scott, B. Shalchi Amirkhiz, I. Pushkareva, Challenges with design and processing of carbide-free bainitic AHSS sheets, in: Proceedings International Symposium On New Developments in Advanced High Strength Sheet Steels, Keystone Colorado, 30th May–2 June, 2017.
[34] J. Huang, W.J. Poole, M. Militzer, Austenite formation during intercritical annealing, Metall. Mater. Trans. A 35A (2004) 3363–3375.
[35] M.J. Roberts, W.S. Owen, Solid solution hardening by carbon and nitrogen in ferrous martensites, in: Physical Properties of Martensite and Bainite, Special Report 93, The Iron and Steel Institute, London, 1965, pp. 171–178.
[36] F.M. AlAbbasi, Predicting the effect of ultrafine ferrite on the deformation behaviour of DP-steels, Comput. Mater. Sci. 119 (2016) 90–107.
[37] M. Calcagnotto, Y. Adachi, D. Ponge, D. Raabe, Deformation and fracture mechanisms in fine- and ultrafine-grained ferrite/martensite dual-phase steels and the effect of aging, Acta Mater. 59 (2011) 658–670.
[38] M.D. Taylor, K.S. Choi, X. Sun, D.K. Matlock, C.E. Packard, L. Xu, F. Barlat, Correlations between nanoindentation hardness and macroscopic mechanical properties in DP980 steels, Mater. Sci. Eng. A 597 (2014) 431–439.
[39] E.J. Garboczi, Geometrical percolation threshold of overlapping ellipsoids, Phys. Rev. E 52 (1) (1995) 819–828.